

Experimentally probing the three-body predissociation dynamics of the low-lying Rydberg states of H₃ and D₃

Christopher M Laperle, Jennifer E Mann, Todd G Clements
and Robert E Continetti¹

Department of Chemistry and Biochemistry, University of California, San Diego,
9500 Gilman Drive, La Jolla, CA 92093-0340, USA

E-mail: rcontinetti@ucsd.edu

Abstract. Charge-exchange neutralization of H₃⁺ with Cs allows preparation of the low-lying Rydberg states of H₃. These states are predissociated by the repulsive ground state and may play roles as intermediates in the dissociative recombination of H₃⁺ + e⁻. Translational spectroscopy and measurements of product momentum partitioning in three-body dissociative charge exchange of fast (12 keV) H₃⁺ and D₃⁺ with Cs yields insights into the nuclear motion during dissociation for the three lowest-lying 2s ²A₁' , 2p ²A₂" and 3p ²E' bound Rydberg states of H₃ and the two 2s ²A₁' and 2p ²A₂" states for D₃. This data provide an empirical benchmark for the refinement of theoretical models involving non-adiabatic interactions and dynamics for H₃.

H₃⁺ is a stable ion that plays a central role in the chemistry of the interstellar medium [1]. Thus, there has been an intense interest in processes related to the destruction and formation of H₃⁺ and the coupling of this ionic species to the chemistry of neutral species. In particular, the dissociative recombination (DR) of H₃⁺,



is thought to be the primary means of H₃⁺ destruction in diffuse interstellar clouds [2]. Experimental and theoretical agreement on the value of the H₃⁺ DR rate coefficient k_{DR} has been a question of intense interest in recent years [3]. An important aspect of the DR process are the dynamics of the excited Rydberg states of H₃. While DR is often mediated by capture to highly excited Rydberg states converging to the ground or low-lying rovibrational states of the cation, an understanding of the dynamics of the lowest lying Rydberg states is of interest from a fundamental perspective. In this work, we study the three-body dissociation processes exhibited by the three lowest long-lived Rydberg states of H₃. Preparation of the Rydberg states by charge exchange of H₃⁺ with Cs and three-body translational spectroscopy is used to examine the three-body dissociation dynamics of these states.

While great strides have been made recently in the convergence of theoretical predictions and experimental results for the value of k_{DR} , there has been little effort devoted to understanding the three-body dissociation dynamics of neutralized H₃⁺. Recently, two groups utilizing fast (MeV) ion beams in

¹ To whom any correspondence should be addressed.

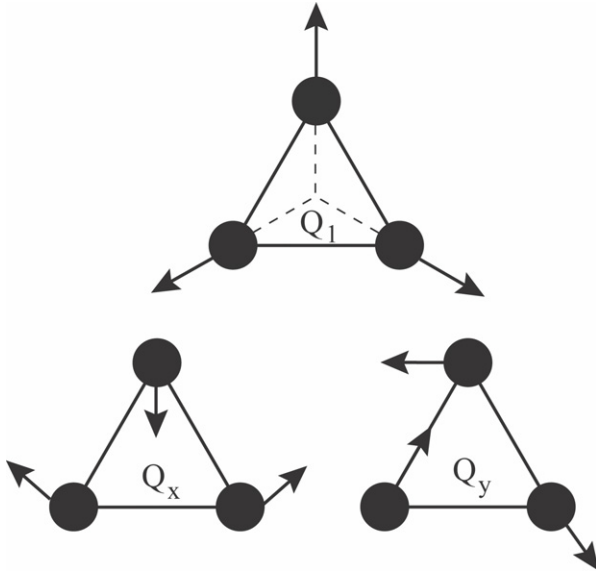


Figure 1. The equilibrium nuclear configuration and distortions due to the normal vibrational modes of H_3 : The symmetric mode Q_1 preserving C_{3v} symmetry and the degenerate modes Q_x and Q_y preserving C_{2v} and C_s symmetry, respectively. Reprinted figure with permission from [13] C M Laperle, J E Mann, T G Clements and R E Continetti, *Phys. Rev. Lett.* **93** 153202 (2004). Copyright (2004) by the American Physical Society.

storage rings have undertaken direct measurements of k_{DR} . Strasser *et al.* have shown that earlier storage ring experiments produced H_3^+ with high rotational temperatures [4]. McCall *et al.* conducted a study with an ion source designed to efficiently cool these rotations and determined $k_{\text{DR}} = 2.7 \times 10^7 \text{ cm}^3 \text{ s}^{-1}$ [5], consistent with the recent theoretical treatment of Kokoouline *et al.* [6,7]. The first study of the three-body dissociation dynamics of DR has recently been reported by Strasser *et al.* using the Heidelberg ion storage ring [8]. In slower keV-energy ion beams much more detailed measurements of three-body dissociation dynamics are possible, as evidenced by the reports of Helm and co-workers on the high-lying Rydberg states and for selected $n = 3$ Rydberg states [9,10,11,12]. The data presented here reports direct measurements of the three-body dissociation dynamics of the three lowest $2s \ ^2A_1'$, $2p \ ^2A_2''$ and $3p \ ^2E'$ Rydberg states of H_3 and complimentary data on the $2s \ ^2A_1'$ and $2p \ ^2A_2''$ Rydberg states of D_3 [13].

The ground state geometry of H_3^+ is an equilateral triangle with C_{3v} nuclear symmetry (see figure 1). The neutral potential energy surfaces (PESs) important in H_3 DR are the ground state surface on which the $\text{H} + \text{H}_2$ reaction occurs and a series of Rydberg states with D_{3h} electronic symmetry. The lone dissociative state in this energy range, the ground $2p \ ^2E'$ state, provides the primary route to dissociation. While Kokoouline *et al.* have shown that even the high lying Rydberg states can couple effectively to the dissociative states, the lower-lying Rydberg states are known to be efficiently predissociated by the $2p \ ^2E'$ state [14]. This dissociative state undergoes a Jahn-Teller distortion, splitting the degenerate surfaces into upper and lower repulsive sheets as the nuclei are distorted from C_{3v} symmetry. These sheets correspond to the three- and two-body dissociation limits respectively [15]. The coupling between the Rydberg states and the upper sheet of the $2p \ ^2E'$ dissociative state governs three-body dissociation. Examining directly the partitioning of momentum in three body dissociation processes can provide insights into the nuclear motion and non-adiabatic couplings between the Rydberg states and the three-body dissociation continuum. At low levels of vibrational excitation, the motion of the nuclei is governed by the normal vibrational modes shown in Figure 1. Evidence for involvement of these normal modes in the coupling between the Rydberg states and the three-body continuum will be presented in this report.

The Rydberg states of H_3 were produced by resonant and near-resonant charge exchange (CE) of a fast (12 keV) H_3^+ ion beam with Cs vapor:



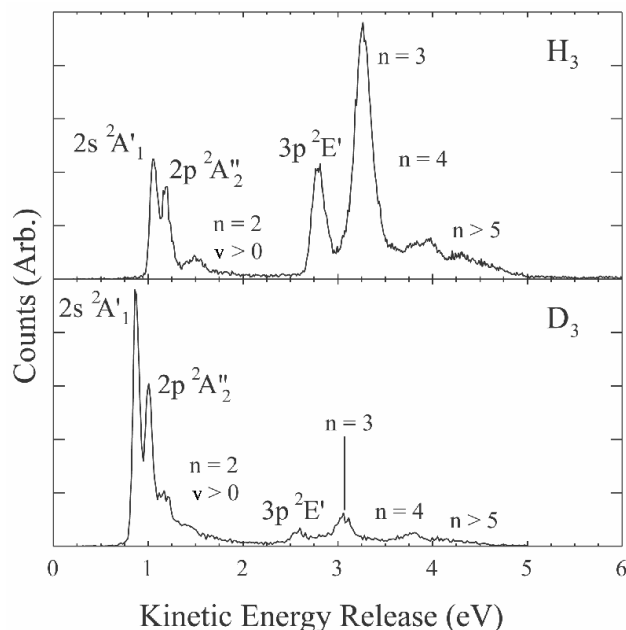


Figure 2. The center-of-mass (CM) kinetic energy release distribution from the three-body dissociation of metastable H_3^* and D_3^* at 12 keV (labels are state assignments). Reprinted from [13] with permission from the AIP.

The states of H_3 formed are determined by both resonant and non-resonant charge-transfer processes. At low relative energies, CE is dominated by resonant processes, however the cross-section for non-resonant CE (NRCE) increases considerably with relative velocity [16]. Since the transitions occur on time scales much faster than nuclear motion, the internal rotational and vibrational state of the cation is strongly preserved in the neutral product [17] and little or no momentum is transferred to the product Cs^+ cation. The resulting fast neutral may be formed in a number of electronically excited Rydberg states of H_3 with geometries similar to H_3^+ .

In this experiment, multi-particle coincidence translational spectroscopy was used to study the dissociation dynamics of transient H_3 formed in the dissociative charge exchange (DCE) of fast H_3^+ with Cs. Products of the dissociation of a single H_3 molecule were detected in coincidence using a multi-particle detector, yielding fragment recoil energies and angular correlations. The experimental approach, using a modified version of an existing spectrometer [18], is briefly reviewed here.

The H_3^+ cation beam was formed from a discharge between two apertures in front of a pulsed (1 kHz) supersonic expansion of pure H_2 or a 10:1 Ar: H_2 mixture. Substitution of D_2 for H_2 allowed generation of D_3^+ and other isotopomers. Experiments on the DCE of O_2^+ indicate that the ions were vibrationally cold ($T_{vib} < 300$ K), with rotational temperatures ≈ 30 K. The ions were skimmed, accelerated to 12 keV and re-referenced to ground potential by a high-voltage switch. The cations were mass-selected by time-of-flight, mass-gated and electrostatically guided through a $\sim 10^{-5}$ torr Cs vapor cell with a path length of ~ 1 mm and a total interaction volume of ~ 1 mm³.

After formation of a metastable neutral by charge transfer of H_3^+ with Cs, dissociation occurred via both the two- and the three-body pathway. Products of DCE recoiled out of the ion beam axis over a 1 m flight length and impinged on a time- and position-sensitive multi-particle detector [18]. This detector consisted of a set of 4-cm diameter microchannel plates in front of four separate delay-line anodes. Each quadrant allowed detection of up to two fragments per dissociation event, allowing up to eight particles to be measured in coincidence per event. The position and time-of-arrival was measured for each fragment, allowing a complete three-dimensional kinematic description of both two- and three-body dissociation events. Given the parent mass, cation beam energy and fragment mass ratio, momentum conservation was checked and the center-of-mass (CM) translational energy and product recoil angles were calculated for each event. The neutral detector was calibrated with the well-known 1 and 3 eV features from DCE of O_2^+ with Cs [19].

The three-body CM kinetic energy release (KER) spectra for H_3 and D_3 are shown in figure 2. Since the three-body dissociation yields only ground state (2S) atomic fragments, the resolved KER

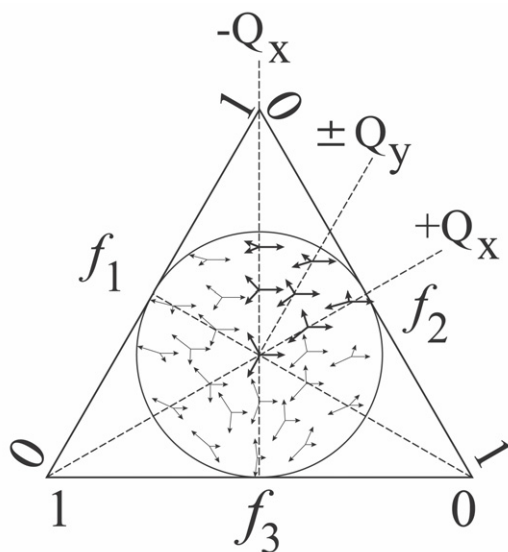


Figure 3. The Dalitz plot represented as a map of the momentum partitioning among the three atomic fragments. The correlation with the asymmetric normal vibrations of H_3 is highlighted in one-sixth of the plot. The f_i are the fractional square of the momentum per particle: $f_i = p_i^2 / \sum p_i^2$. Reprinted from [13] with permission from the AIP.

spectra reflect the discrete energy levels of the low-lying Rydberg states of H_3 and D_3 . As the density of states increases with increasing energy, unresolved features at high KER are observed for the manifolds of $n = 3$ and $n \geq 4$ states. Even though the $n \geq 3$ states are off resonance by ~ 2 -5 eV, they are still efficiently populated via NRCE. These spectra also exhibit a feature associated with vibrational excitation of the $n = 2$ Rydberg states, possibly due to initial vibrational excitation in the cation beam. Comparison of the H_3 and D_3 KER spectra shows that, as expected, NRCE plays a larger role for H_3 because of its higher relative velocity. The lowest rotational level of the $2p \ ^2A_2''$ state is long-lived (≈ 640 ns) [20] therefore the data assigned to the $2p \ ^2A_2''$ state of H_3 must arise from a state with some rotational excitation

Since the lowest Rydberg states are resolved in the three-body KER spectrum, it is possible to examine the three-body dissociation dynamics in greater detail by selecting a narrow energy range and determining the momentum partitioning among the three H or D atom products. An instructive way of examining the momentum partitioning is to use a Dalitz plot [21]. The Dalitz plot is constructed by plotting the fractional square of the individual fragment momenta as the distance from the side of an equilateral triangle (see figure 3). For equal mass fragments, the triangle represents energy conservation and the inscribed circle represents momentum conservation. The three-body channel results in three atomic fragments, indistinguishable from one another, yielding a Dalitz plot with six-fold degeneracy and three-fold symmetry. Each point in the Dalitz plot corresponds to a different partitioning of the product momenta thus allowing visualization of the fragment CM momentum partitioning [10,14]. Figure 4 shows the Dalitz plot representations for the low-lying Rydberg states of H_3 and D_3 . Figure 4(F) shows the results of a Monte Carlo simulation of the geometric detector collection efficiency at KER = 2.7 eV (the KER of the $H_3 \ 3p \ ^2E'$ state), showing that the multiparticle detection scheme samples most three-body dissociation geometries equally. The collection efficiency for a KER of 1 eV, not shown, is nearly unity for all geometries of H_3 or D_3 . Since there is no significant attenuation in the raw data, none of the data presented here has been corrected for detector collection efficiency.

The correlation between the normal modes shown in figure 1 and the momentum partitioning in the Dalitz plot should hold for prompt dissociation of triatomic hydrogen near the symmetric D_{3h} configuration and in the absence of significant exit channel interactions among the three H atom products. As shown in figure 3, the $+Q_x$ coordinate corresponds to distortion from equilateral C_{3v} to a linear configuration via a C_{2v} nuclear motion. This distortion asymptotically leads to two particles with large momenta and one with a near-zero momentum. The $-Q_x$ coordinate corresponds to a C_{2v} distortion correlating with perpendicular insertion of H into an H_2 bond, as shown by the three-body

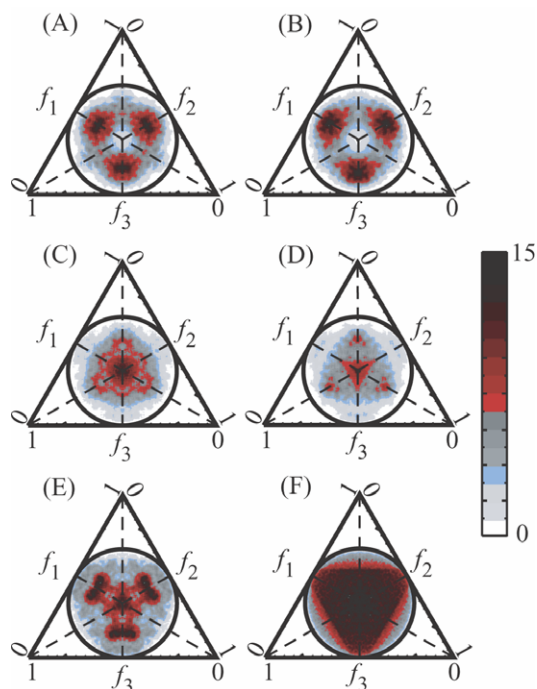


Figure 4. (color online) The Dalitz plot representations for (A-B) $2s\ ^2A_1'$ in H_3 and D_3 , (C-D) $2p\ ^2A_2''$ in H_3 and D_3 , (E) $3p\ ^2E'$ in H_3 and (F) a Monte Carlo simulation of the detection efficiency at $KER = 2.7$ eV. The axis labels f_i are the fractional square of momentum partitioning ($f_i = p_i^2/\sum p_i^2$). The scale is linear from 0-15, normalized to the most intense features in each plot. Reprinted from [13] with permission from the AIP.

dissociation kinematic model of Maul and Gericke [22]. Motion along the $\pm Q_y$ coordinate corresponds to asymmetric momentum partitioning along the bisector of the angle made by the $\pm Q_x$ axes, while motion along Q_1 , the symmetric vibration, will lead to equal momentum partitioning and be observed as a feature at the center. In the next sections, energy selected Dalitz plots are presented for each of the low-lying Rydberg states. These plots are generated by only analyzing events that occur with the appropriate KER range for a given state. The rotational distribution of the states formed in the CE process is a direct reflection of the rotational distribution in the cation beam. To that extent, the narrow widths of the peaks in the KER reveal that the rotational distribution of the neutrals formed is not very significant.

Figure 4(A-B) shows the Dalitz plots for predissociation of the $2s\ ^2A_1'$ states of H_3 and D_3 . These Dalitz plots were obtained by analyzing events where the KER was in the range 1.00–1.12 eV and 0.75–0.92 eV for H_3 and D_3 , respectively. Both systems exhibit a high-density feature off-center along the $+Q_x$ axis indicating that only a restricted range of nuclear configurations undergo facile crossing to the repulsive surface. The location of this feature indicates that the $2s\ ^2A_1'$ and upper sheet of the dissociative $2p\ ^2E'$ states interact when the nuclei are distorted towards linear geometry. The coupling of the $2s\ ^2A_1'$ and $2p\ ^2E'$ states must occur via vibronic interactions of the degenerate (Q_x and Q_y) vibrations of e' symmetry [23]. The data presented here only arises from dissociation of the ground vibrational state of $2s\ ^2A_1'$ H_3 and D_3 , therefore the coupling to the $2p\ ^2E'$ state occurs via zero-point vibrational motion along the $+Q_x$ coordinate. Within the Born-Oppenheimer approximation the PESs are identical for H_3 and D_3 , thus the subtle isotope effect must arise from the smaller amplitude zero-point wavefunction for D_3 .

Figure 4(C-D) shows the Dalitz plots for events corresponding to the predissociation of $2p\ ^2A_2''$ H_3 and D_3 . These Dalitz plots were obtained by analyzing events where the KER was in the range 1.12–1.35 eV and 0.92–1.08 eV for H_3 and D_3 , respectively. Both systems exhibit a high-density feature at the center and features along the symmetry axes spreading into the asymmetric region. The center feature indicates that dissociation is most favorable near the symmetric C_{3v} configuration, corresponding to nuclear motion along the Q_1 coordinate. This result is consistent with Herzberg's assertion that the $2p\ ^2A_2''$ state rotationally couples to the $2p\ ^2E'$ state [24]. The initial C_{3v} nuclear configuration is not expected to significantly distort with rotational motion thereby yielding totally symmetric momentum partitioning among the fragments. The weaker off-center features are not as

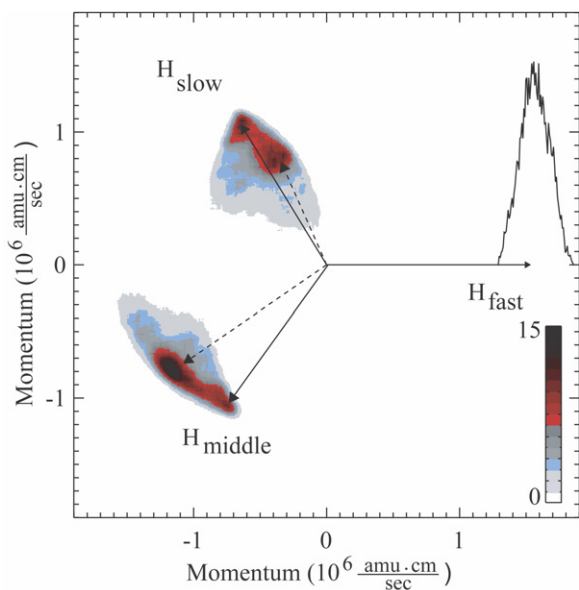


Figure 5. (color online) The molecular-frame differential cross-section for the dissociation of $3p\ ^2E'$ H_3 (see text for details).

prominent and show an isotope effect. H_3 exhibits weak features away from the center and along both the $\pm Q_x$ axes. The dissociation of D_3 with a $\pm Q_x$ nuclear distortion is markedly different. The D_3 data also shows a feature corresponding to a $-Q_x$ distortion, however it is broader and more pronounced than for H_3 . In addition, a weak feature is also observed far out along the $+Q_x$ distortion direction, corresponding to dissociation of a near-linear D_3 molecule. No feature corresponding to a near-linear distortion of this magnitude is observed for H_3 .

Figure 4(E) shows the Dalitz plot for predissociation of the $3p\ ^2E'$ state of H_3 , generated from analyzing the events in the KER range 2.60-3.00 eV. This state is also resolved for D_3 , however insufficient data was obtained to generate a useful Dalitz plot owing to the reduced population of this state by NRCE at the beam energy of 12 keV. Galster *et al.* have recently reported a study of the three-body dissociation of the $3p\ ^2E'$ state of H_3 using a different method of preparation [12]. More specifically, the lowest rotational level of the long-lived $2p\ ^2A_2''$ state, prepared via CE between H_3^+ and Cs, was optically excited to the $3d\ ^2E''$ state which undergoes spontaneous emission, yielding the $3p\ ^2E'$ state. The data from the laser studies and those presented in figure 4(E) are similar. High-density features are observed in both the central symmetric region and slightly off the $+Q_x$ axis. Low density is observed directly along the $+Q_x$ axis, splitting the feature near the $+Q_x$ axis in half.

In addition to the Dalitz plot, the molecular frame differential cross-section (MF-DCS) is also a useful means for visualizing three-body dissociation mechanisms. The MF-DCS is generated by plotting the CM momentum distribution of a reference particle along the x-axis and the momentum vector distributions of the other two fragments relative to the reference particle in the plane of the three-body breakup [25]. The MF-DCS for the dissociation of $3p\ ^2E'$ H_3 is shown in figure 5 where the fastest H-atom fragment is chosen as the reference particle. Two regions of high density are evident, indicated by the solid and dashed arrows, and point to the peak momentum distributions for dissociation of the totally symmetric and asymmetric H_3 , respectively.

The $3p\ ^2E'$ state is doubly degenerate and thus subject to a Jahn-Teller distortion. The complicated fragment momentum distribution associated with the predissociation of the $3p\ ^2E'$ state must be a direct result of Jahn-Teller effects. An intriguing possibility is that the dominant totally symmetric and asymmetric features in the Dalitz plot, connected by a path between them, may indicate that three-body dissociation competes with the Jahn-Teller distortion in the nascent $3p\ ^2E'$ state. Kokoouline and Greene have calculated the PES for the doubly degenerate $3p\ ^2E'$ state and the resulting Jahn-Teller surfaces for fixed values of the Q_1 symmetric stretch normal mode [14]. The lower surface has three minima, two have configurations involving distortions characterized by $(-Q_x \pm Q_y)$ and one is along the $+Q_x$ axis. A possible mechanism for the three-body dynamics is that immediately after CE, the nuclear

configuration has C_{3v} symmetry and begins to undergo Jahn-Teller distortion on the PES toward the lower sheet minima, however three-body dissociation competes with the distortion at all times. The high-density regions of the momentum partitioning indicated in the Dalitz plot and in the MF-DCS in Figure 5 may thus trace the evolution of the nuclei as three-body predissociation occurs along the path to the minima. The asymmetric feature in the Dalitz plot correlates qualitatively with the calculated minimum on the $+Q_x$ axis except for the low-density of data directly on the $+Q_x$ axis. Another possibility is that there are two distinct geometries that couple to the three-body continuum, a symmetric and a distorted one. Given the > 60 ps radiative lifetime found for asymmetric-stretch-excited levels of the $3p \ ^2E'$ state [26], this is certainly possible for the vibrationless levels as well, although it is not clear that the system could effectively sample the symmetric configuration after Jahn-Teller distortion.

In conclusion, this data demonstrates the unique and complex three-body dissociation dynamics of the low-lying Rydberg states of H_3 and D_3 . The D_3 results indicate an observable isotope effect on the three-body dissociation mechanism of these states. These experimental results provide valuable information for evaluating theoretical models of H_3^+ DR and the non-adiabatic dynamics of the excited electronic states of H_3 and D_3 . As seen in Helm's presentation at the 6th International Conference on Dissociative Recombination, complementary results on the states discussed here have been obtained, and the agreement is striking. In these experiments, the Rydberg states are prepared by spontaneous emission from laser-excited higher-lying states. This confirms that we now have the means to provide detailed differential cross sections for the three-body decay of simple molecules, and will hopefully promote a new generation of theoretical efforts to understand these complicated dynamical processes.

This work was supported by the US Air Force Office of Scientific Research under grants F49620-03-1-0039 and FA9550-04-1-0035. We thank Dr. Morton A. Fineman for his contributions to this research.

References

- [1] Watson W D 1973 *Astrophys. J.* **183** L17
- [2] Oka T 2003 *Dissociative Recombination of Molecular Ions with Electrons* ed S Guberman (New York: Kluwer, Plenum) p 209
- [3] Larsson M 2000 *Philos. Trans. R. Soc. London A* **358** 2433
- [4] Strasser D, Lammich L, Kreckel H, Krohn S, Lange M, Naaman A, Schwalm D, Wolf A and Zajfman D 2002 *Phys. Rev. A* **66** 032719
- [5] McCall B J *et al.* 2003 *Nature* **422** 500
- [6] Kokoouline V, Greene C H and Esry B D 2001 *Nature* **412** 891
- [7] Kokoouline V and Greene C H 2003 *Phys. Rev. Lett.* **90** 133201
- [8] Strasser D *et al.* 2001 *Phys. Rev. Lett.* **86** 779
- [9] Müller U and Cosby P C 1999 *Phys. Rev. A* **59** 3632
- [10] Müller U, Eckert T, Braun M and Helm H 1999 *Phys. Rev. Lett.* **83** 2718
- [11] Galster U, Kaminski P, Beckert M, Helm H and Müller U 2001 *Euro. Phys. J. D* **17** 307
- [12] Galster U, Müller U and Helm H 2004 *Phys. Rev. Lett.* **92** 073002
- [13] Laperle C M, Mann J E, Clements T G and Continetti R E 2004 *Phys. Rev. Lett.* **93** 153202
- [14] Kokoouline V and Greene C H 2003 *Phys. Rev. A* **68** 012703
- [15] Petsalakis I D, Theodorakopoulos G and Wright J S 1988 *J. Chem. Phys.* **89** 6850
- [16] Sidis V and de Bruijn D P 1984 *Chem. Phys.* **85** 201
- [17] Spalburg M R, Los J and Gislason E A 1985 *Chem. Phys.* **94** 327
- [18] Hanold K A, Luong A K, Clements T and Continetti R E 1999 *Rev. Sci. Instr.* **70** 2268
- [19] van der Zande W J, Koot W, Peterson J R and Los J 1987 *Chem. Phys. Lett.* **140** 175
- [20] Bordas C, Cosby P C and Helm H 1990 *J. Chem. Phys.* **93** 6303
- [21] Dalitz R H 1953 *Philos. Mag.* **44** 1068
- [22] Maul C and Gericke K-H 2000 *J. Phys. Chem. A* **104** 2531
- [23] Dabrowski I and Herzberg G 1980 *Can. J. Phys.* **58** 1238
- [24] Herzberg G, Hougen J T and Watson J K G 1982 *Can. J. Phys.* **60** 1261
- [25] Luong A K, Clements T G and Continetti R E 1999 *J. Phys. Chem. A* **103** 9190